Cellular and Molecular Bioengineering, Vol. 10, No. 1, February 2017 (© 2016) pp. 3–15
DOI: 10.1007/s12195-016-0469-0

A Microfluidic Model of Hemostasis Sensitive to Platelet Function and Coagulation

R. M. Schoeman,[1] K. Rana,[1] N. Danes,[2] M. Lehmann,[1] J. A. Di Paola,[3] A. L. Fogelson,[4] K. Leiderman,[3] and K. B. Neeves[1,3]

[1]Chemical and Biological Engineering Department, Colorado School of Mines, 1500, Illinois St, Golden, CO 80401, USA; [2]Applied Mathematics and Statistics Department, Colorado School of Mines, Golden, CO, USA; [3]Department of Pediatrics, University of Colorado Denver, Aurora, CO, USA; and [4]Departments of Mathematics and Bioengineering, University of Utah, Salt Lake City, Utah, USA

(*Received 14 June 2016; accepted 12 October 2016; published online 24 October 2016*)

Associate Editor Michael R. King oversaw the review of this article.

Abstract—Hemostasis is the process of sealing a vascular injury with a thrombus to arrest bleeding. The type of thrombus that forms depends on the nature of the injury and hemodynamics. There are many models of intravascular thrombus formation whereby blood is exposed to prothrombotic molecules on a solid substrate. However, there are few models of extravascular thrombus formation whereby blood escapes into the extravascular space through a hole in the vessel wall. Here, we describe a microfluidic model of hemostasis that includes vascular, vessel wall, and extravascular compartments. Type I collagen and tissue factor, which support platelet adhesion and initiate coagulation, respectively, were adsorbed to the wall of the injury channel and act synergistically to yield a stable thrombus that stops blood loss into the extravascular compartment in ~ 7.5 min. Inhibiting factor VIII to mimic hemophilia A results in an unstable thrombus that was unable to close the injury. Treatment with a P2Y12 antagonist to reduce platelet activation prolonged the closure time two-fold compared to controls. Taken together, these data demonstrate a hemostatic model that is sensitive to both coagulation and platelet function and can be used to study coagulopathies and platelet dysfunction that result in excessive blood loss.

Keywords—Biorheology, Biotransport, Platelets, Coagulation.

INTRODUCTION

Hemostasis is the physiological process by which a vascular injury is sealed by the formation of a blood clot, or thrombus, while maintaining vessel patency. There are numerous *in vitro*[26] and *in vivo*[53] models of intravascular thrombus formation, which is relevant to thrombotic events such as those following atherosclerotic plaque rupture.[36] Yet, there are relatively few models of extravascular thrombus formation, which is relevant to bleeding diatheses and trauma. The objective of this study is to develop an *in vitro* model of extravascular thrombus formation that captures the salient feature of hemostasis; namely a reliance on platelet function and coagulation to plug a hole in a vessel under physiological pressure gradients.

Hemostasis consists of two connected processes, platelet function and coagulation, which are triggered when injury exposes blood to the vascular wall and extravascular space. Platelet deposition begins when platelets adhere to collagen[9] and other extracellular matrix proteins. The adherent platelets become activated, secrete platelet-activating chemicals such as ADP from their granules into the surrounding fluid, and recruit more platelets to bind and form a platelet plug to prevent initial blood leakage.[15] This initial formation of a platelet plug is referred to as primary hemostasis. Coagulation can be initiated by tissue factor (TF) in the extravascular space; it progresses by means of enzymatic reactions on the surfaces of activated platelets.[24] A major product of coagulation is thrombin which promotes earlier reaction steps to accelerate its own production, activates platelets, and converts the soluble plasma protein fibrinogen into insoluble fibrin that polymerizes to form a stabilizing mesh surrounding the platelet mass.[51] The stabilization of the initial platelet plug with fibrin is referred to as secondary hemostasis. The mechanisms of platelet adhesion and aggregation and the relative role of platelet function and coagulation are regulated by forces

Address correspondence to K. B. Neeves, Chemical and Biological Engineering Department, Colorado School of Mines, 1500, Illinois St, Golden, CO 80401, USA. Electronic mail: kneeves@mines.edu

R. M. Schoeman and K. Rana contributed equally to this study.

and mass transfer limitations imposed on a growing thrombus by blood flow.[10,35]

In normal hemostasis, numerous competing biophysical and biochemical processes are properly balanced and a plug is formed that stops the bleeding but does not block blood flow through the damaged vessel.[50] This balance can be disrupted in many ways. In particular, deficiencies of the clotting factors VIII, IX, and XI, known as hemophilia A, B, and C, respectively, results in bleeding in muscles and joints.[44] Deficiencies in von Willebrand factor (VWF), known as von Willebrand disease (VWD), reduce platelet adhesion leading to mucocutaneous bleeding, and in some cases bleeding into the gastrointestinal tract.[6] Similar bleeding patterns observed as in VWD are found in individuals with low platelet counts (thrombocytopenia) or platelet function disorders. Reliably predicting the consequences of these deficiencies is not yet possible, in part, due to a lack of *in vitro* models of hemostasis that incorporate the forces induced by blood flow on a growing thrombus.

In vitro flow-based assays of intravascular thrombus formation have been vital for measuring the shear stress dependent mechanisms associated with platelet adhesion and aggregation and mass transfer regulation of coagulation.[13,35,37,43] In the typical flow assay, whole blood is perfused through a parallel plate flow chamber over adhesive surfaces consisting of one or a combination of extracellular matrix proteins such as collagen, von Willebrand factor, laminin, fibrinogen, and fibronectin.[7,16,38,49] The most common substrate is type I collagen, which is found in the vascular wall and is a strong platelet agonist and initiator of the intrinsic pathway of coagulation *via* activation of factor XII.[22,46] Immobilized TF is used to introduce the extrinsic pathway, which tends to result in a higher concentration of thrombin and more pronounced fibrin deposition.[28,31,32] These assays are typically performed at a constant flow rate to achieve a desired wall shear rate. However, they can also be performed at a constant pressure gradient to achieve channel occlusion.[2,5] Advances in microfluidics have allowed for more complex flow chamber designs[26] that include features like a stenosis,[19,41,52] endothelialized networks that mimic the microvasculature,[40,42,55] and porous walls that model the vessel wall.[25]

The biophysical regulation of intravascular and extravascular thrombus formation is potentially different due to differences in geometry, fluid dynamics, and the biochemical environment between the intravascular and extravascular space, as well as clinical observations of location and duration of bleeds in individuals with hemophilia and VWD. The size of an intravascular clot is constrained by the vessel size. Whereas, extravascular spaces include large cavities such as the joints and gastrointestinal tract, where bleeding from hemophilia and VWD are common.[29,44] Arterial and venous thrombosis occurs in large vessels, where inertial forces dominate the hemodynamics, whereas bleeding in genetic bleeding disorders occurs in the microvasculature where viscous forces dominate. The levels of coagulation proteins and their inhibitors are different in the intravascular and extravascular space. For example, synovial fluid contains high levels of small coagulation factors such as factors IX and XI, but less than 1% of plasma levels of larger factors V and VIII.[4] TF is undetectable in endothelial cells, but expressed at high levels in cells of the medial layer of blood vessels.[8]

In this study, we present a model of hemostasis where a small channel representing a vascular injury is sealed by thrombus. The injury channel was coated with type I collagen and TF to mimic components that are found in the vascular wall and promote platelet adhesion and coagulation, respectively. A constant pressure difference across the injury was used to mimic physiological intravascular pressures. Inhibition of either platelet function or coagulation resulted in prolonged closure times or unstable thrombi.

MATERIALS AND METHODS

Materials

Bovine serum albumin (BSA), calcium chloride, magnesium chloride, sodium chloride, potassium chloride, disodium phosphate, dipotassium phosphate, HEPES, methanol, hydrochloride acid (37 N), $DiOC_6$, methanol, and 2-Methylthioadenosine 5′-monophosphate triethylammonium (2-MeSAMP) were obtained from Sigma Aldrich (St. Louis, MO, USA). SYLGARD® 184 Silicone Elastomer Kit was purchased form Dow Corning (Midland, MI, USA). Relipidated recombinant human tissue factor (TF) was purchased from Innovin® Dade-Behring (Miami, FL). Equine type I fibrillar collagen was purchased from Chrono-Log Corporation (Havertown, PA). Murine anti-human FVIII antibody (clone GMA-8015) was purchased from Green Mountain Antibodies (Burlington, VT). KMPR 1050 and KMPR 1010 were purchased from MicroChem Corporation (Westborough, MA). Human fibrinogen was purchased from Enzyme Research Laboratory (South Bend, IN) and labeled with Alexa-555 labeling kit purchased from Life Technologies (Grand Island, NY). 10X HEPES Buffered Saline (HBS) was prepared by dissolving 1500 mM NaCl and 250 mM HEPES in deionized (18.2 MΩ-cm) water. 10X HBS was diluted to 1X using deionized water prior to use.

Recalcification buffer was prepared by dissolving 75 mM $CaCl_2$ and 35 mM $MgCl_2$ in HBS. 2% BSA solution was prepared by dissolving 1 g of BSA in 50 mL of 1X HBS. Wash buffer was HBS with 3.2% sodium citrate. All buffers were adjusted to a pH of 7.4 using 1 M HCl and 1 M NaOH and filtered through a 0.22 μm pore size syringe filter (Millipore, Billerica, MA) prior to use. Stock buffers were stored at 4 °C until use. Buffers were allowed to equilibrate to room temperature before use.

Microfluidic Device Design and Fabrication

The master template for the device was prepared with KMPR 1010 and KMPR 1050 photoresists to define a two-layer device with heights of 20 μm and 50 μm. PDMS was molded off of these masters using standard soft lithography procedures. The PDMS was exposed to an oxygen plasma and bonded to glass slides cleaned in 1:1 12 M HCl:methanol for 1 h and rinsed with 18.2 MΩ-cm deionized water and subsequently dried at 80 °C for 4 h. The device was designed in the shape of the letter 'H' where the outer two vertical channels represent the vascular and extravascular compartments (10 mm long × 100 μm wide × 50 μm high), respectively. The vertical channels are connected by a horizontal channel (150 μm long × 50 μm wide × 20 μm high) representing a hole in the vessel wall, which we refer to hereafter as the injury channel (Figs. 1a, 1c, and 1d). Type I fibrillar collagen, recombinant human TF, or a combination of the two were adsorbed to the walls of the injury channel by introducing 10 μL of solution through the inlet of the extravascular channel while the blood channel contained only air. Using a pipet, negative pressure was applied at the outlet of the extravascular channel to pull the solution into the device. Applying fluctuating pressure with the pipet at the blood channel outlet, the injury channel was then filled. The solution was contained in the injury channel due to capillary forces at solution-air interface between the injury channel and the blood channel. BSA (2% in HBS), collagen, TF or collagen-TF solutions were allowed to adsorb on the walls of the injury channel at 4 °C for 12 h. Prior to introduction of blood, the mixer and blood channel were blocked with 2% BSA in HBS for 1 h.

Blood Collection and Preparation

Blood was collected from healthy donors by venipuncture into vacutainer tubes containing 3.2% sodium citrate in keeping with common practices for flow assays including coagulation.[28] Donors had not consumed alcohol within 48 h prior to the draw, nor had they taken any prescription or over-the-counter drugs within the previous 10 days excluding oral contraception. The first tube of blood collected was treated as waste to eliminate any activated platelets due to venipuncture. Platelet counts and hematocrits were measured and recorded for each donor. In cases where the platelet counts were lower than 150,000/μL, the samples were discarded due to potential activation of platelets while drawing blood. 960 μL aliquots of blood collected in sodium citrate was combined in tubes with 40 μL of Alexa-555 labeled fibrinogen (final concentration 56 μg/mL) which was added to visualize fibrin deposition. Platelets were labeled with the lipophilic dye $DiOC_6$ (1 μM final concentration). Labeled platelets were incubated at 37 °C in the presence or absence of 12 nM anti-FVIII antibody or 100 μM the P2Y12 antagonist 2-MeSAMP for 15 min prior to the assay.

Device Operation

Figure 1a shows the schematic of the fluidic network. Pressure was controlled for the blood, recalcification buffer, and wash buffer (3.2% sodium citrate in HBS) independently by applying a pressure to the headspace of their respective reservoirs using a pressure-based flow controller (Fluigent MFCS, Villejuif, France). Blood was recalcified in the ratio of 9:1 (citrated whole blood:recalcification buffer) using a herringbone mixer.[15,18] The output from the herringbone mixer was connected to the blood channel of the extravascular injury device using a 50 cm length of 0.25 mm ID Tygon tubing. The pressures of the blood and recalcification reservoirs were held constant at 10 kPa. The wash buffer reservoir was connected to the extravascular channel by 18 cm of 0.5 mm ID tubing connected to 60 cm of 0.25 mm ID Tygon tubing. The different tubing diameters were necessary to make connections to the reservoir and microfluidic device. The pressure in the wash buffer was initially set to 3.5 kPa to drive a small amount of wash buffer through the injury channel while the blood channel was filled with recalcified blood driven by 10 kPa of pressure in the blood and recalcification reservoirs. The pressure in the wash reservoir was then reduced to 1.75 kPa so that the blood passes from the blood channel into the injury channel and out into the extravascular channel. Thrombus formation was monitored through an inverted microscope (IX81, Olympus) equipped with a 16 bit CCD camera (Hamamatsu, San Jose, CA) using relief contrast and epifluorescence microscopy with a 20× objective (NA 0.45) for up to 45 min. Time to closure was defined as the first time that no red blood cells (RBC) pass through the injury channel for 5 s. The kinetics of platelet and fibrin accumulation in the injury channel were calculated by measuring the integrated

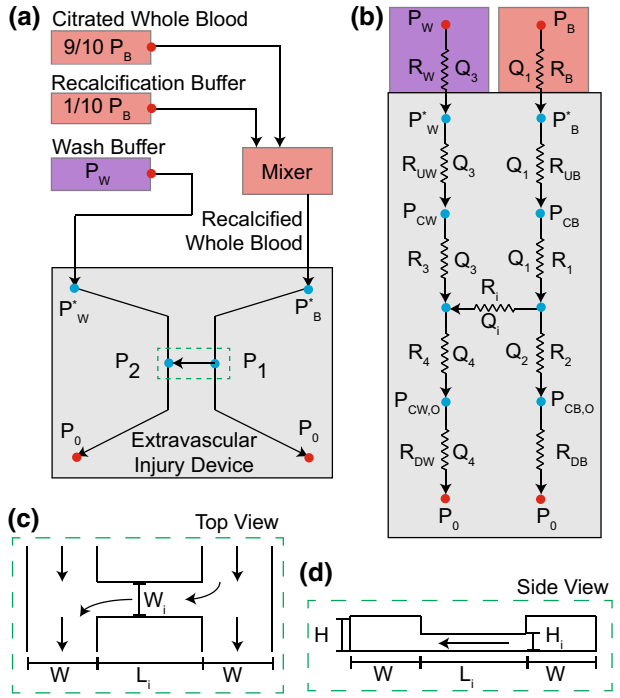

FIGURE 1. (a) Schematic of the fluidic network and extravascular injury device. The pressure in reservoirs containing citrated whole blood, recalcification buffer, and wash buffer was defined using an off-chip pressure controller. The citrated whole blood and recalcification buffer were combined in a microfluidic herringbone mixer at a 9:1 volumetric flow rate ratio. The recalcified whole blood and wash buffer were introduced into two vertical channels in the extravascular injury device. A horizontal 'injury' channel connects the two vertical channels. Red and blue dots indicate user-defined and calculated pressures, respectively. (b) The hydraulic resistance network that includes resistances of tubing, the mixer, and the microfluidic channels in the extravascular injury device. (c, d) Zoomed in top and side views at the intersection of the vertical channels and horizontal channel. All dimensions, pressures, resistances, and flow rates are found in Tables 1, 2, and 3.

fluorescence intensity in the injury channel for each frame using ImageJ.[24,39]

Hydraulic Circuit Analysis

Pressures and flow rates in the fluid network were calculated using hydraulic circuit analysis where hydraulic resistances were arrayed in series and parallel as outlined in Fig. 1b and in the Supplemental Material. Resistances in off-chip tubing was calculated by[30]:

$$R = \frac{8\mu L}{\pi r^4} \tag{1}$$

where μ is the dynamic viscosity, L is the length, and r is the inner radius. Resistances in each channel of the extravascular injury device were calculated by[30]:

$$R = \frac{a\mu L}{wh^3} \tag{2}$$

where L is the length, w is the width, and h is the height of the channel and a is defined as:

$$a = 12\left[1 - \frac{192h}{\pi^5 w}\tanh\left(\frac{\pi w}{2h}\right)\right]^{-1} \tag{3}$$

The resistance through the mixer was determined by measuring the flow rate through the mixer at a pressure of 10 kPa in the both the whole blood and recalcification buffer reservoirs.

Computational Fluid Dynamics

Flow through the device was simulated by numerically solving the incompressible Navier–Stokes equations in three dimensions using a projection method. We used the rotational incremental pressure-correction scheme[14] with Taylor–Hood elements for the spatial discretization and a BDF-2 time discretization. With this method, the convergence for the velocity is second order in space and order-3/2 in time, while the pressure is first order in both space and time. Each vertical channel of the computational domain is 150 μm long and connected on one face center to the injury channel (Fig. 2a). An unstructured mesh consisting of ~50,000 tetrahedral elements was generated with Gmsh.[12] The flow was pressure-driven with specified pressures at the inlets and outlets of the vertical channels. The computational domain simulates only a small segment of the device thus, to obtain the pressures, we used the hydraulic resistance network calculations described below. The fluid solver was written in-house, using the FEniCS v.1.6 software suite.[20] We used passive tracer particles to monitor flow behavior through the injury channel. A spherical source of 40,000 passive tracer particles with 28 μm diameter was placed near in the blood channel upstream of the injury channel and particles were monitored as they traversed through the injury channel. Post-processing, passive tracer particle integration, and visualization were done in ParaView v.5.0.1.[1] In order to reduce the computational cost of simulating fluid flow through the device, we only modeled the vertical channels 75 μm upstream and 75 μm downstream of the horizontal channel. To determine the pressure boundary conditions at the ends of the vertical segments, each vertical channel was divided into four resistors in series; P_{CW} and P_{CB} are the pressures in the wash and blood channel 75 μm upstream of the horizontal channel, and $P_{CW,O}$ and $P_{CB,O}$ are the pressures in the wash and blood channel 75 μm downstream of the horizontal channel. The circuit analysis solution gives these four pressures which are then used in the flow simulations.

were calculated using hydraulic circuit analysis (Fig. 1b). The known pressures were those in the headspace of the citrated whole blood, recalcification buffer, and wash buffer reservoirs, and the outlet pressure of each vertical channel. The hydraulic resistances through the tubing attaching the reservoirs to the device and through the rectangular channels of the device were calculated using Eqs. 1–3. Tables 2 and 3 summarizes the resistances depicted in Fig. 2b and the calculated pressures and flow rates. This fluidic network is different than typical flow assays that include a single channel with inlet and outlet tubing because of the dynamics of the flow as the injury channel approaches occlusion. For the equivalent geometries and inlet and outlet pressures, the normal force on the thrombus is at least half that in the 'H' geometry compared to a straight channel (see Supplemental Fig. 1 and Supplemental Material for calculations). Further, convective mass transfer dominates at the interface of an occlusive thrombus in the 'H' geometry because flow in the blood channel is unimpeded. In contrast, the flow rate in the straight channel approaches zero and mass transfer to the interface is primarily diffusive (assuming an impermeable thrombus). Therefore, in the 'H' geometry a thrombus is exposed to a higher transport rate of new plasma proteins and blood cells as the injury channel approaches, and following, occlusion.

The velocity, wall shear rate, and pressure distributions were calculated using finite element method simulations for the region of the device near the injury channel prior to significant accumulation of platelet or fibrin (Fig. 2). The calculated average wall shear rate on the bottom wall of the horizontal, injury channel is 10,900 s^{-1} for a pressure drop of 873 Pa. The width of the tracer particle stream in the computational extravascular channel is comparable to the width of the whole blood in the physical device's extravascular channel under the same inlet pressures suggesting that these simulations model the appropriate flow rates, and consequently the initial wall shear rates and pressures in the injury channel (Fig. 3).

Table 4 gives the geometric and dynamic parameters that characterize flow, mass transfer and heterogeneous enzymatic reactions in the injury channel per the recommendation of the ISTH Biorheology Subcommittee.[23] The Reynolds number is slightly less than unity, suggesting that viscous forces dominate over inertial forces. Flow is fully developed through the majority of the injury channel as the entrance length is less than one micrometer. The Peclet number is large, and consequently mass transfer in dominated by convective transport. There are many binding and enzymatic reactions occurring simultaneously, but with the relatively large mass transfer coefficient and thus small concentration boundary layer, we anticipate most reactions will be reaction-limited.[35] As one example, the conversion of factor X to factor Xa by the TF:FVIIa complex has a Dahmköhler number much less than unity, which is in the reaction-limited regime.

TABLE 1. Extravascular injury device channel dimensions.

Height of vertical channels, H	50 μm
Height of horizontal channel, H_i	20 μm
Width of vertical channels, W	100 μm
Width of horizontal channel, W_i	50 μm
Length of vertical channels, L	10 mm
Length of horizontal channel, L_i	150 μm

TABLE 2. Hydraulic resistances corresponding to the resistance network in Fig. 1b.

R_B	6.00×10^{13} Pa s/m^3
R_W	2.56×10^{13} Pa s/m^3
R_{UB}, R_{UW}, R_{DB}, R_{DW}	2.75×10^{13} Pa s/m^3
R_1, R_2, R_3, R_4	4.19×10^{11} Pa s/m^3
R_i	2.40×10^{13} Pa s/m^3

TABLE 3. Calculated pressures and flow rates from hydraulic resistance network in Fig. 1b.

Reservoir pressure, blood, P_B	10.0 kPa
Reservoir pressure, wash, P_W	1.75 kPa
Inlet pressure, blood, P^*_B	4.41 kPa
Inlet pressure, wash, P^*_W	1.45 kPa
Inlet pressure computational domain, blood, P_{CB}	1.85 kPa
Inlet pressure computational domain, wash, P_{CW}	1.13 kPa
Outlet pressure computational domain blood, P^*_{CB}	1.78 kPa
Outlet pressure computational domain wash, P^*_{CW}	1.11 kPa
Pressure drop across horizontal injury channel, P_1–P_2	0.68 kPa
Inlet flow rate, blood, Q_1	9.32×10^{-11} m^3/s
Outlet flow rate, blood, Q_2	6.47×10^{-11} m^3/s
Inlet flow rate, wash, Q_3	1.17×10^{-11} m^3/s
Outlet flow rate, wash, Q_4	4.02×10^{-11} m^3/s
Injury flow rate, Q_i	2.85×10^{-11} m^3/s

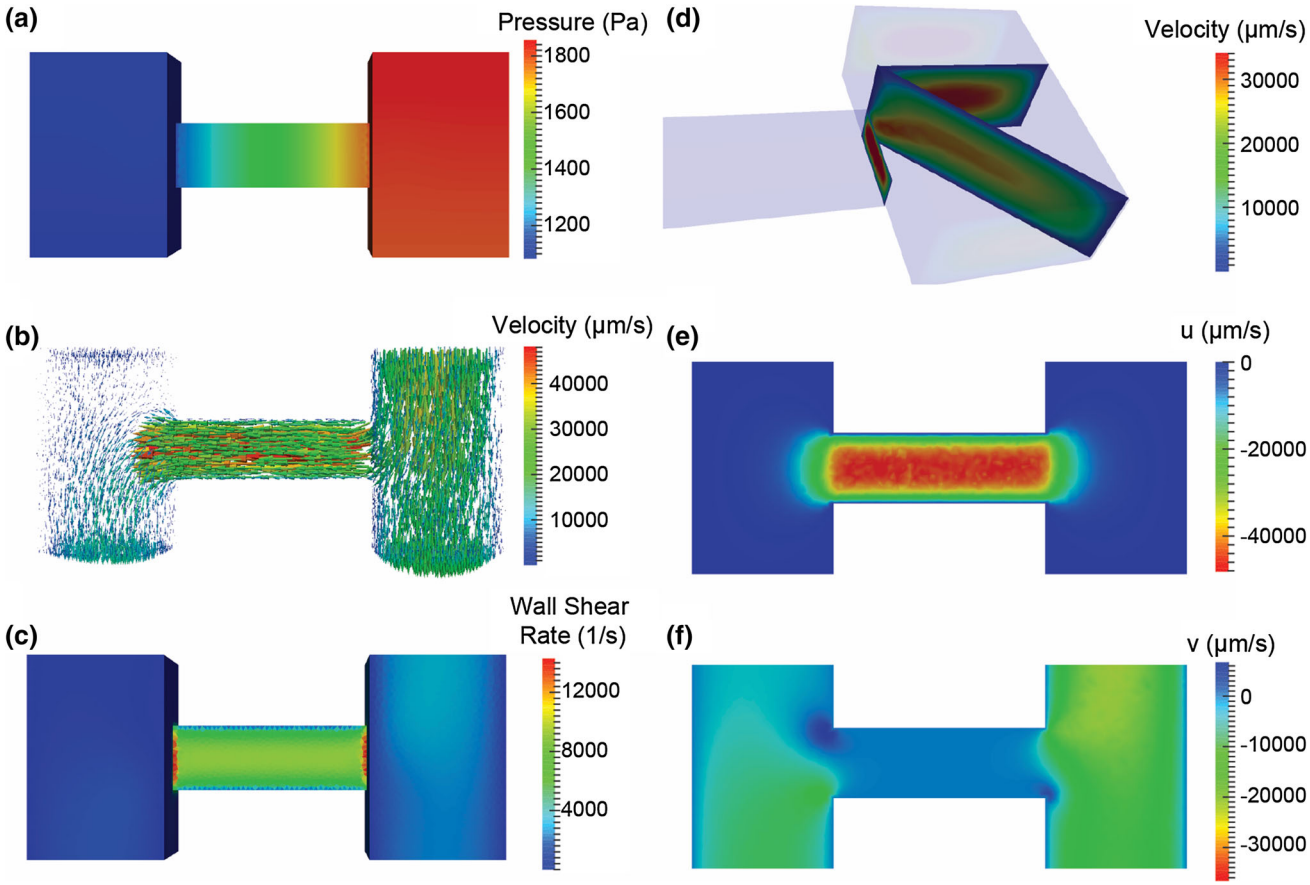

FIGURE 2. Top down view of the pressure (a), velocity (b), and wall shear rate (c) distributions in the vascular channel (right), extravascular channel (left) and horizontal injury channel from computational solution of the Navier–Stokes equations. Magnitude of the velocity in the z-plane (d) at two locations in the vascular channels and one location at the inlet of the injury channel. Slices through the *x–y* plane at the half-height of the injury channel showing the *x*-component (e) and *y*-component (f) of the velocity.

Statistical Analysis

Differences in closure times for different conditions were compared using a Mann–Whitney *U*-test for $n = 4$ donors. Time to closure is represented as the mean ± standard deviation.

RESULTS

Device Characterization

The device has an 'H' geometry consisting of two vertical channels connected to one another by a horizontal channel where whole blood and sodium citrate are perfused through the two parallel vertical channels that are connected to each other by a horizontal channel (Figs. 1a, 1c, and 1d). One vertical channel represents the vascular compartment, and the other represent the extravascular compartment, and the horizontal channel represents a vascular injury. The citrated whole blood and recalcification buffer were combined at a volumetric ration of 9:1 with a herringbone mixer to yield a physiological concentration of divalent cations.[18] Recalcified whole blood and wash buffer were perfused through the vascular and extravascular channels, respectively. The absolute pressure (P_B) of the citrated whole blood and recalcification buffer were adjusted to give an average wall shear rate of 2200 s^{-1} in the blood channel, which is within the range of wall shear rates in human arterioles.[17] During initial filling of the blood channel, the hematocrit is low and approaches a constant value as indicated by reduced light transmission in bright field microscopy. During this initial filling period the pressure of the wash buffer (P_W) was initially set so that wash buffer flows through the injury channel until a constant blood flow was achieved. Then, P_W is reduced such that blood flows through the injury. Tables 1 and 3 contain the dimensions of the device and the operating conditions used in this study.

The pressure drop across the horizontal channel and the inlet and outlet pressures for CFD simulations

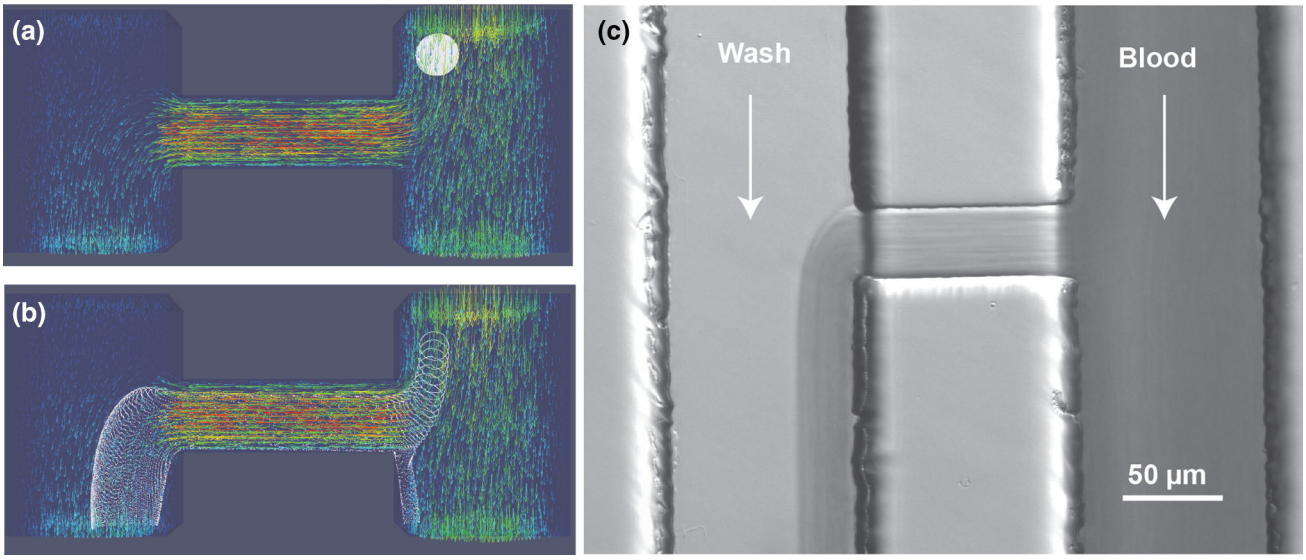

FIGURE 3. (a) and (b) A spherical source of 40,000 passive tracer particles placed near the inlet of the injury channel at $t = 0$ (a) and their particle distribution after $t = 0.5$ ms (b). (c) Bright field image of whole blood in the extravascular injury device for $P_B = 10$ kPa and $P_W = 1.75$ kPa.

TABLE 4. Parameters that characterize the geometry and flow, mass transfer, and reaction regimes in the injury channel.

Parameter	Expression	Value	Constants
Aspect ratio	H/W	0.4	$H = 20\ \mu$m, $W = 50\ \mu$m
Relative injury size	L/H	7.5	$H = 20\ \mu$m, $L = 150\ \mu$m
Reynolds number (R_e)	$\rho UH/\mu$	0.4	$\rho = 1060$ kg/m^3, $U = 2.8 \times 10^{-2}$ m/s, $H = 20\ \mu$m, $\mu = 1.6 \times 10^{-2}$ Pa s *
Entrance Length (L_e)	0.05 ReD_h**	0.6 μm	$D_h = 28\ \mu$m
Peclet number (P_e)	$\gamma H^2/6D$ †	7.3×10^5	$\gamma = 10{,}900\ s^{-1}$, $H = 20\ \mu$m, $D = 10^{-11}$ m^2/s
Mass transfer coefficient (k_m)	$(D^2\gamma/8L)^{1/3}$	9.6×10^{-6} m/s	$D = 10^{-11}$ m^2/s, $\gamma = 10{,}900\ s^{-1}$, $L = 150\ \mu$m
Dahmköhler number (D_a)†	$k_{cat}C_E/k_m - C_S$ ‡	7×10^{-2}	$k_{cat} = 1.15\ s^{-1}$, $C_E = 10$ fmol/cm^2, $C_S = 0.17\ \mu$M

H height of channel, W width of channel, L length of channel, U average blood velocity, D diffusivity, γ wall shear rate, k_{cat} rate constant, C_E enzyme surface concentration, C_S substrate concentration. *Viscosity estimated from empirical relationship for blood flow in tubes with diameters <1 mm.[34] **D_h, hydraulic diameter [2HW/(H + W)]. †Approximate diffusivity of coagulation proteins.[54] ‡Calculated using k_{cat} for the conversion of FX to FXa by TF:FVIIa complex where, C_E is the concentration of TF:FVIIa complex, C_S is the plasma concentration of FX.[21] Surface concentration of TF from Onosaga-Jarvis *et al.*[32]

Collagen and TF Act Synergistically to Yield a Mechanically Stable Thrombus

The vessel wall contains a complex milieu of adhesive and procoagulant proteins that support thrombus formation. Here, we use type I collagen, a strong platelet agonist and adhesive ligand for platelets *via* the glycoprotein VI and $\alpha_2\beta_1$ receptors, and/or TF, the initiator of the extrinsic pathway of coagulation and considered their effect on the time to closure of the injury channel (Fig. 4). Channels coated with BSA did not support platelet adhesion or significant fibrin deposition suggesting that velocity gradients at the entrance and exit of the injury channel do not promote thrombus formation in the absence of agonist (Supplementary Video 1). Type I collagen alone supports platelet adhesion and fibrin accumulation in the near-wall region underneath platelet aggregates. Initial thrombus formation is dictated by the position of collagen fibers in the injury channel and not fluid dynamics in this model (Supplemental Fig. 2). There was no consistent location for initial platelet adhesion in the channel for collagen or collagen-TF surfaces. However, as the thrombus approaches closure, platelet aggregates embolize, and full closure is not achieved over 45 min. TF alone leads to initial fibrin formation in the corners of the injury channel followed by platelet adhesion to the deposited fibrin. The time to closure of the horizontal channel is 15.8 ± 2.0 min. Type I collagen and TF together support platelet accumulation and fibrin formation with a time to occlusion of 7.5 ± 1.6 min. On the combined collagen-TF surface, platelets first adhere and aggregate to form a plug in

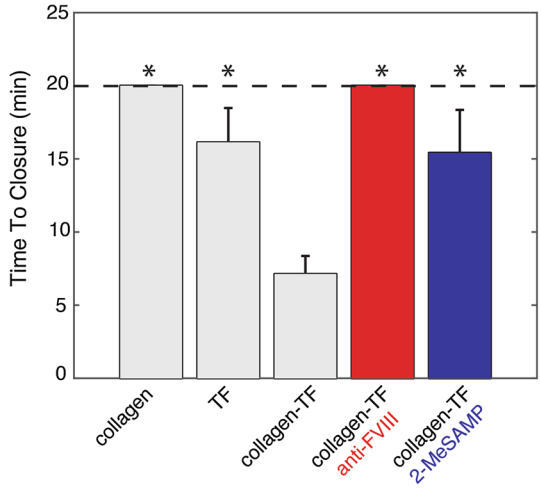

FIGURE 4. The effect of prothrombotic substrate, simulated FVIII deficiency, and anti-platelet agent on time to closure of the injury channel. Surfaces (gray bars) considered were type I collagen, TF, and type I collagen and TF together. For simulated FVIII deficiency (red bar) blood was treated with an anti-FVIII antibody. The P2Y12 antagonist 2-MeSAMP (blue bar) was used as an anti-platelet agent. Conditions that reach the dotted line did not close. An asterisk denotes a significant difference ($p < 0.01$) between the untreated whole blood on the collagen-TF surface and other conditions.

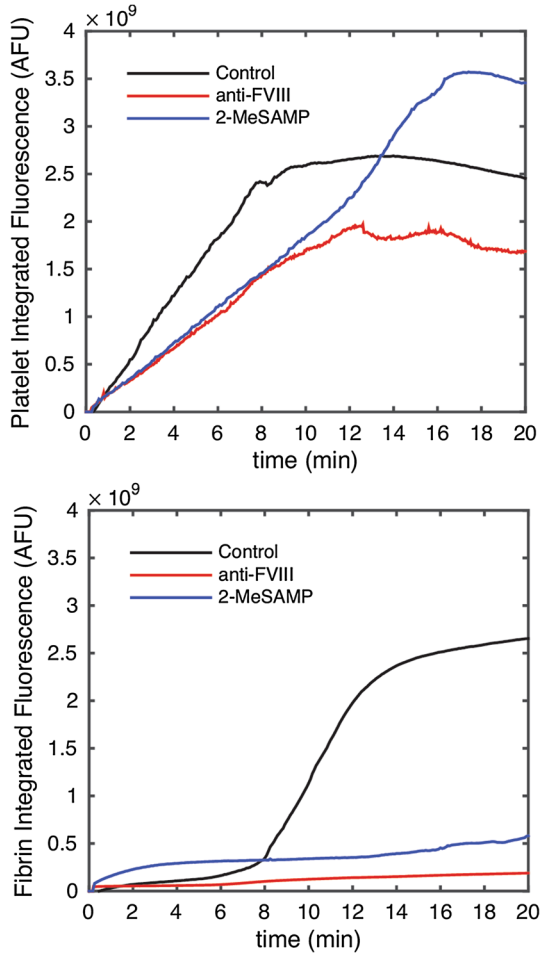

FIGURE 5. Characteristic platelet and fibrin accumulation in the injury channel for whole blood on collagen-TF (control) and whole blood treated with an anti-FVIII antibody or the P2Y12 antagonist 2-MeSAMP. The integrated fluorescence intensity in the injury channel is expressed in arbitrary fluorescent units (AFU).

the injury channel that stops the loss of blood into the extravascular compartment (Fig. 5, Supplemental Video 2). Fibrin was observed within the dense platelet plug, particularly in the near-wall region. Following cessation of flow, fibrin rapidly polymerizes across the entire horizontal channel (Figs. 5 and 6). These data demonstrate that collagen and TF act synergistically to form a stable thrombus whereby both primary hemostasis (formation of a platelet plug) and secondary hemostasis (stabilization by fibrin) are necessary.

Inhibition of FVIII Results in Unstable Thrombi Unable to Close the Injury

Normal whole blood treated with a function blocking anti-human FVIII antibody did not form stable thrombi (Fig. 7). Initial platelet accumulation was similar to that for the collagen-TF surface with untreated blood (Fig. 5), however, as the thrombus approached closure large aggregates of platelets were shed, a process that was repeated several times over the duration of the experiment (Supplementary Video 3). After 30 min there was only modest increases in platelet accumulation and blood continued to leak through the channel for up to 45 min. Fibrin accumulation was significantly reduced compared to controls and limited to the near-wall region where large platelet aggregates were attached likely protecting coagulation products from dilution by flow (Fig. 5).

Inhibition of P2Y12 Receptor Prolongs Closure Time and Leaky Thrombi

Normal whole blood treated with the P2Y12 antagonist 2-MeSAMP resulted in a prolonged time to closure (15.2 ± 3.4 min) compared to untreated blood on collagen-TF surfaces (Fig. 4). The platelet plug was larger in area than in untreated whole blood, typically filling the entire horizontal channel, and took longer to accumulate than for the untreated blood (Figs. 5 and 8). Thrombi appeared less compact and contained less fibrin, potentially due to reduced platelet activation, and were less mechanically stable than in untreated blood as indicated by the displacement of large platelet aggregates in the direction of flow (Supplemental Video 4). Importantly,

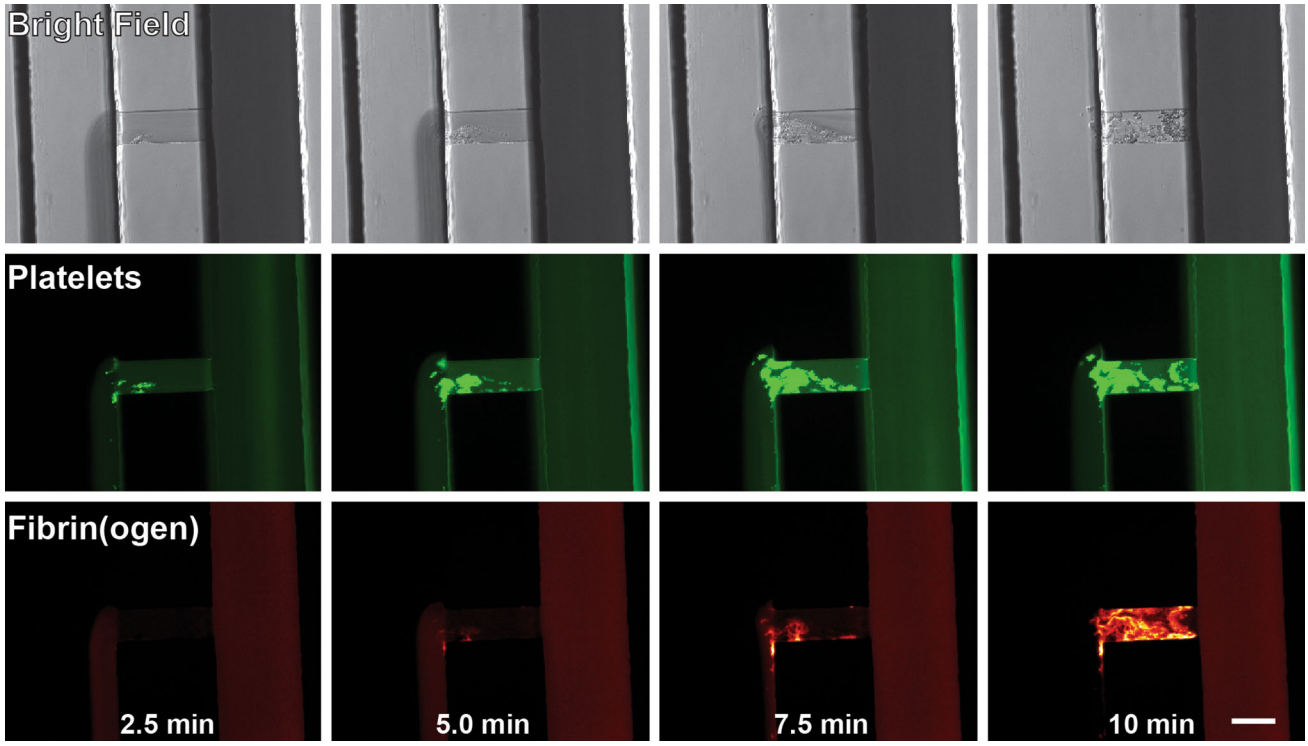

FIGURE 6. Time course of thrombus formation on a collagen-TF surface with recalcified citrated whole blood. Time to closure was 8 min. Blood (right channel) and wash buffer (left channel) flow from top to bottom and through the horizontal injury channel. Platelets are labeled with $DiOC_6$ and fibrino(gen) is labeled with Alexa-555. Scale bar = 50 μm.

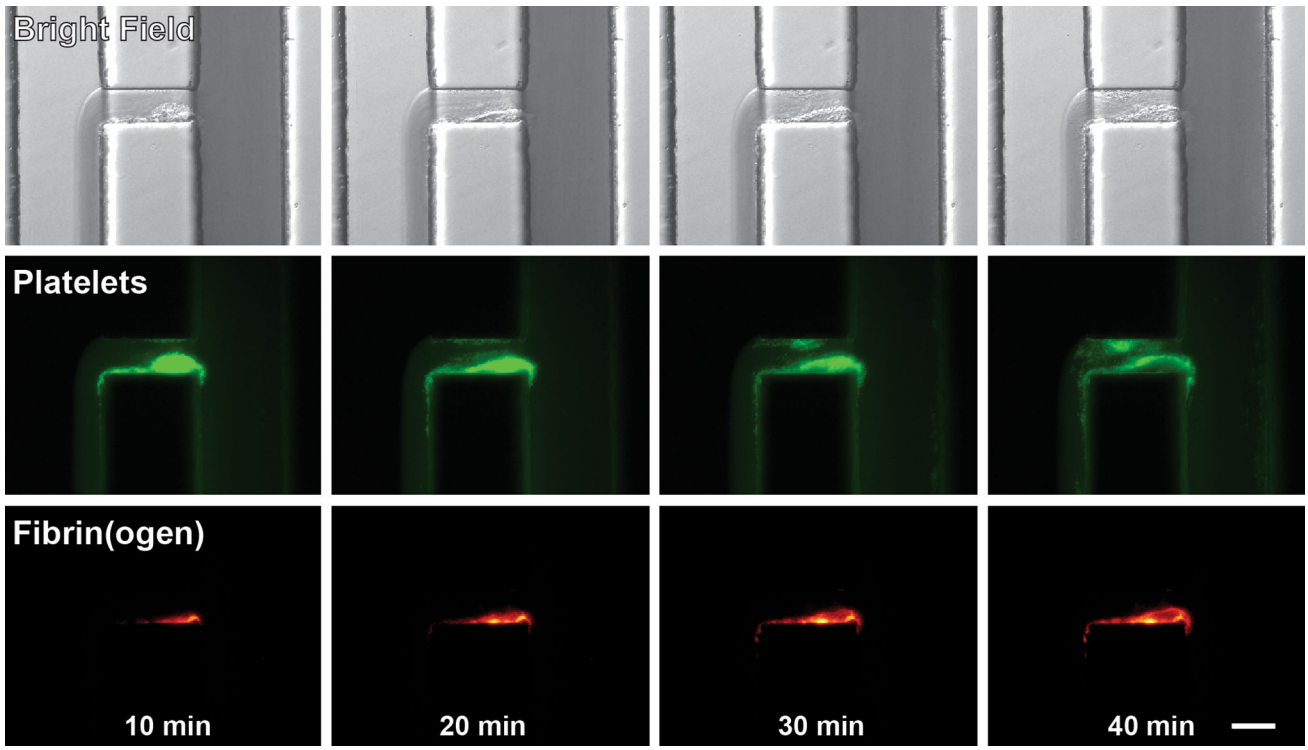

FIGURE 7. Time course of thrombus formation on a collagen-TF surface with recalcified citrated whole blood treated with an anti-FVIII antibody. A stable thrombus did not form to close the injury channel over 45 min. Blood (right channel) and wash buffer (left channel) flow from top to bottom and through the horizontal injury channel. Platelets are labeled with $DiOC_6$ and fibrino(gen) is labeled with Alexa-555. Scale bar = 50 μm.

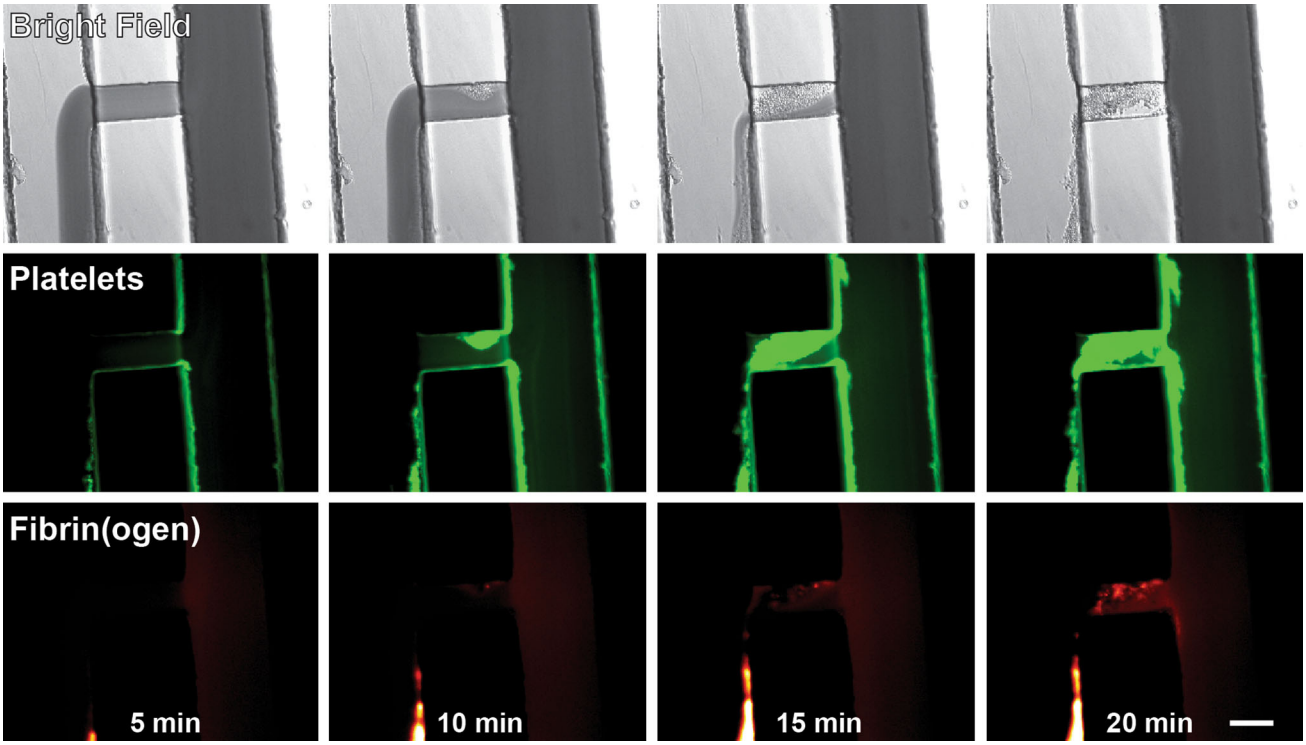

FIGURE 8. Time course of thrombus formation on a collagen-TF surface with recalcified citrated whole blood treated with the P2Y12 antagonist 2-MeSAMP. Time to closure was 16 min. Blood (right channel) and wash buffer (left channel) flow from top to bottom and through the horizontal injury channel. Platelets are labeled with $DiOC_6$ and fibrino(gen) is labeled with Alexa-555. Scale bar = 50 μm.

following closure as defined the arrest of red blood cells moving across the injury channel, we continued to observe leakage of plasma indicating a porous thrombus. No such leakage was observed in untreated controls.

DISCUSSION

Hemostasis is a function of blood flow, platelet function, and coagulation. In this study, we describe a microfluidic model of hemostasis that depends on all three of these phenomena. Most *in vitro* flow models consist of flowing blood over a prothrombotic substrate resulting in a thrombus that grows into the lumen of a channel. These models are a suitable representation of thrombosis. Here, a thrombus forms in a small side channel to arrest extravasation of blood from one channel into another in a process that better represent hemostasis. This geometry provides two unique features compared to conventional flow models. First, there are two paths for blood flow—through the injury channel or the blood channel—that are controlled independently. As a result, as the injury channel occludes, the flow rate through the blood channel remains unchanged, and importantly, continues to deliver plasma proteins and blood cells to the periphery of the thrombus. Second the normal force is smaller in an extravascular injury compared intravascular injury for comparable pressure gradients and channel geometries. Hemostasis by platelet deposition did not appear to be consistent with any fluid mechanics parameter in this model. The sizes of the channels are comparable to the microvasculature in humans where the majority of bleeds occur in genetic bleeding disorders such as hemophilia, VWD, or platelet disorders. The wall shear rate in the blood channel and the pressure drop across the injury channel are comparable to those found in the arterioles.[33] Normal whole blood in a collagen-TF coated injury channel recreates primary and secondary hemostasis with the initial formation of a platelet plug that is then stabilized with fibrin. The time to closure of the injury depends on both FVIII and autocrine signaling through the ADP receptor P2Y12, with deficits in either resulting in prolonged closure times and unstable or leaky thrombi.

The geometry of the injury channel controls whether platelet-surface or platelet–platelet interactions dominate. For the geometry of our channel with height of 20 μm and aspect ratio of 0.4, we would expect platelet-surface interactions to dominate based on the criteria of Casa and Ku, especially at early times.[3] However, at late times as the thrombus approaches occlusion the role of platelet–platelet interaction in

clearly important based on the prolonged closure time in experiments with a P2Y12 antagonist.

Our microfluidic hemostasis model yields qualitatively similar results as some animal models of hemostasis. Getz and colleagues described a murine model of hemostasis that operates on the same principles as our microfluidic device.[11] Here, a laser ablation is used to create a 50–100 μm diameter hole in the saphenous vein. Mice with platelet function defects in the form of *talin1* or GP1bα deficiencies could not achieve hemostasis. Inhibition of P2Y12 with clopidogrel resulted in ~50% increase in occlusion time, similar to our results with the P2Y12 antagonist 2-MeSAMP that yielded an approximately two-fold increase in closure time. Mice expressing low levels of TF or deficient in FIX had similar initial closure times as wild type controls, but the thrombi were unstable upon repeated laser injury. We did not observe closure in the absence of TF or when inhibiting FVIII activity with a function blocking antibody. These data suggest that our model is perhaps more dependent on coagulation that this murine model. Van Gestal and colleagues use a micropipette to create a 6–8 μm injury in the arterioles of rabbits.[47] Similar to our model, use of ADP receptors antagonists still allow for the formation of a hemostatic plug, however that plug is more prone to rebleeding, which is consistent with our observation of a leaky, porous thrombus.[48] The time scale for closure is significantly longer in our microfluidic model (minutes) than in these animal models (tens of seconds). There are several explanations for this discrepancy. First, the injury size in the rabbit arteriole model is significantly smaller than our injury channel. Second, the microenvironment *in vivo* includes endothelial and vascular wall cells that play an active role in promoting thrombus formation. For example, activated endothelial cells secrete large multimers of VWF that can form a net to catch platelets. Moreover, the vessel wall contains VWF, while in our model only plasma VWF is present. The adsorption of plasma VWF to type I collagen determines the lag time for platelet adhesion under flow.[27] Third, in our device blood components are washed away from the injury in the extravascular channel, which in the animal models they may accumulate in the extravascular space.

The device presented here is more dependent on coagulation than platelet function for the formation of stable thrombi. Inhibition of FVIII leads to mechanically unstable clots that could not close the injury channel over 45 min. Similarly, collagen surfaces without TF did not lead to closure. These results are in agreement with those in a microfluidic model of intravascular thrombus formation where corn trypsin inhibitor treated whole blood is perfused over type I collagen-TF surfaces in a pressure relief mode through a 60 μm high channel.[5] Yet, studies in a micropipette model of intravascular thrombus formation on type I collagen alone yields occlusion times of 17 min for a 200 μm high channel under constant pressure.[2] In a microfluidic model of a stenosed vessel (20-50 μm high at the apex), occlusions on collagen only formed for wall shear rates greater than 4000 s^{-1}.[19] These discrepancies between models likely reflect differences in collagen density density, model injury size, and preparation of prothrombotic substrates, as well as in chamber dimensions and geometry and flow regimes.[23] In the hemostatic model described here we rely on diffusion of large collagen fibrils, often several millimeters in length, into the horizontal injury channel over 12 h. This patterning procedure leads to a significantly lower density of collagen than by convective delivery using microfluidic patterning.[18] A higher density of collagen or other platelet adhesive proteins could provide a surface that was more platelet dependent.

The precise genesis of vascular injuries in genetic and acquired bleeding disorders in humans is largely unknown. There is little data regarding the nature and extent of vascular injury and even the vessels from which blood is lost. Genetically modified animals with deficiencies in coagulation proteins do not exhibit the same bleeding patterns as humans with similar deficiencies. For example, hemophilia A mice do not spontaneously bleed into joints, but rather require blunt trauma to induce bleeds.[45] As such, *in vitro* models such as the one described in this study provide an opportunity to explore the large parameter space that contributes to bleeding including, but not limited to, injury size, hemodynamics, vessel wall composition, and the anatomy of the adjacent perivascular and extravascular spaces. In this study we describe an experimental platform for studying hemostasis with a focus on collagen-TF induced thrombus formation within a model vascular wall. In the current configuration, the platform could be extended to study the effect of extravascular coagulation proteins and the geometry of the extravascular space.

ELECTRONIC SUPPLEMENTARY MATERIAL

The online version of this article (doi:10.1007/s12195-016-0469-0) contains supplementary material, which is available to authorized users.

ACKNOWLEDGMENTS

This work was supported by a NSF CAREER (CBET-1351672), American Heart Association (14GRNT20410094), and the National Institutes of Health (R01HL120728, R21NS082933).

ANIMAL STUDIES

No animal studies were carried out by the authors for this article.

CONFLICT OF INTEREST

The authors R. M. Schoeman, K. Rana, N. Danes, and M. Lehmann declare that they have no conflicts of interest. J. A. Di Paola, A. L. Fogelson, K. Leiderman, and K. B. Neeves reports Grants from NIH and NSF. A. L. Fogelson reports personal fees from Genentech outside the submitted work.

HUMAN SUBJECTS

All procedures followed were in accordance with the ethical standards of the responsible committee on human experimentation (University of Colorado, Boulder) and with the Helsinki Declaration of 1975, as revised in 2000. Informed consent was obtained from all subjects for being included in the study.

REFERENCES

[1]Ayachit, U. The ParaView Guide: A Parallel Visualization Application. New York: Kitware, Inc, 2015.
[2]Berny, M. A., I. A. Patel, T. C. White-Adams, P. Simonson, A. Gruber, S. Rugonyi, and O. J. T. McCarty. Rational design of an ex vivo model of thrombosis. *Cell. Mol. Bioeng*. 3:187–189, 2010.
[3]Casa, L. D. C., and D. N. Ku. Geometric design of microfluidic chambers: platelet adhesion versus accumulation. *Biomed Microdevices* 16:115–126, 2014.
[4]Chang, P., D. L. Aronson, D. G. Borenstein, and C. M. Kessler. Coagulant proteins and thrombin generation in synovial fluid: a model for extravascular coagulation. *Am. J. Hematol*. 50:79–83, 1995.
[5]Colace, T. V., R. W. Muthard, and S. L. Diamond. Thrombus growth and embolism on tissue factor-bearing collagen surfaces under flow: role of thrombin with and without fibrin. *Arterioscl Throm Vas* 32:1466–1476, 2012.
[6]De Jong, A., and J. Eikenboom. Developments in the diagnostic procedures for von Willebrand disease. *J. Thromb. Haemost*. 14:449–460, 2016.
[7]de Witt, S. M., F. Swieringa, R. Cavill, M. M. E. Lamers, R. Van Kruchten, T. Mastenbroek, C. Baaten, S. Coort, N. Pugh, A. Schulz, I. Scharrer, K. Jurk, B. Zieger, K. J. Clemetson, R. W. Farndale, J. W. M. Heemskerk, and J. M. E. M. Cosemans. Identification of platelet function defects by multi-parameter assessment of thrombus formation. *Nat. Commun*. 5:4257, 2014.
[8]Drake, T. A., J. H. Morrissey, and T. S. Edgington. Selective cellular expression of tissue factor in human tissues. Implications for disorders of hemostasis and thrombosis. *Am. J. Pathol*. 134:1087, 1989.
[9]Farndale, R. W., J. J. Sixma, M. J. Barnes, and P. G. de Groot. The role of collagen in thrombosis and hemostasis. *J. Thromb. Haemost*. 2:561–573, 2004.
[10]Fogelson, A. L., and K. B. Neeves. Fluid mechanics of blood clot formation. *Ann. Rev. Fluid Mech*. 47:377–403, 2015.
[11]Getz, T. M., R. Piatt, B. G. Petrich, D. Monroe, N. Mackman, and W. Bergmeier. Novel mouse hemostasis model for real-time determination of bleeding time and hemostatic plug composition. *J. Thromb. Haemost*. 13:417–425, 2015.
[12]Geuzaine, C., and J. F. Remacle. Gmsh: A 3-D finite element mesh generator with built-in pre- and post-processing facilities. *Int. J. Numer. Methods Eng* 79:1309–1331, 2009.
[13]Goldsmith, H. L., and V. T. Turitto. Rheological aspects of thrombosis and haemostasis: basic principles and applications. ICTH-Report-Subcommittee on Rheology of the International Committee on Thrombosis and Haemostasis. *Thromb. Haemost*. 55:415–435, 1986.
[14]Guermond, J. L., P. Minev, and J. Shen. An overview of projection methods for incompressible flows. *Comput. Method Appl. Mech. Eng*. 195:6011–6045, 2006.
[15]Jackson, S. The growing complexity of platelet aggregation. *Blood* 109:5087, 2007.
[16]Jen, C. J., and J. S. Lin. Direct observation of platelet adhesion to fibrinogen- and fibrin-coated surfaces. *Am. J. Physiol*. 261:H1457–H1463, 1991.
[17]Koutsiaris, A. G., S. V. Tachmitzi, and N. Batis. Wall shear stress quantification in the human conjunctival precapillary arterioles in vivo. *Microvasc. Res*. 85:34–39, 2013.
[18]Lehmann, M., A. M. Wallbank, K. A. Dennis, A. R. Wufsus, K. M. Davis, K. Rana, and K. B. Neeves. On-chip recalcification of citrated whole blood using a microfluidic herringbone mixer. *Biomicrofluidics* 9:064106, 2015.
[19]Li, M., D. N. Ku, and C. R. Forest. Microfluidic system for simultaneous optical measurement of platelet aggregation at multiple shear rates in whole blood. *Lab Chip* 12:1355, 2012.
[20]Logg, A., K.-A. Mardal, and G. N. Wells. Automated Solution of Differential Equations by the Finite Element Method. Berlin, Heidelberg: Springer, 2012.
[21]Mann, K. G., M. E. Nesheim, W. R. Church, P. Haley, and S. Krishnaswamy. Surface-dependent reactions of the vitamin K-dependent enzyme complexes. *Blood* 76:1–16, 1990.
[22]Manon-Jensen, T., N. G. Kjeld, and M. A. Karsdal. Collagen-mediated hemostasis. *J. Thromb. Haemost*. 14:438–448, 2016.
[23]McCarty, O. J. T., D. Ku, M. Sugimoto, M. R. King, J. M. E. M. Cosemans, K. B. Neeves. The Subcommittee on Biorheology. Dimensional analysis and scaling relevant to flow models of thrombus formation: communication from the SSC of the ISTH. *J. Thromb. Haemost*. 14:619–622, 2016.
[24]Monroe, D. M., and M. Hoffman. Coagulation factor interaction with platelets. *Thromb. Haemost*. 88:179, 2002.
[25]Muthard, R. W., and S. Diamond. Side view thrombosis microfluidic device with controllable wall shear rate and transthrombus pressure gradient. *Lab Chip* 13:1883–1891, 2013.
[26]Neeves, K. B., A. A. Onasoga, and A. R. Wufsus. The use of microfluidics in hemostasis. *Curr. Opin. Hematol*. 20:417–423, 2013.

[27]Neeves, K. B., A. A. Onasoga, R. R. Hansen, J. J. Lilly, D. Venckunaite, M. B. Sumner, A. T. Irish, G. Brodsky, M. J. Manco-Johnson, and J. A. Di Paola. Sources of Variability in Platelet Accumulation on Type 1 Fibrillar Collagen in Microfluidic Flow Assays. *PLoS One* 8:e54680, 2013.

[28]Neeves, K. B., O. J. T. McCarty, A. J. Reininger, M. Sugimoto, M. R. King. Biorheology Subcommittee of the SSC of the ISTH. Flow-dependent thrombin and fibrin generation in vitro: opportunities for standardization: communication from SSC of the ISTH. *J. Thromb. Haemost*. 12:418–420, 2014.

[29]Nichols, W. L., M. B. Hultin, A. H. James, M. J. Manco-Johnson, R. R. Montgomery, T. L. Ortel, M. E. Rick, J. E. Sadler, M. Weinstein, and B. P. Yawn. von Willebrand disease (VWD): evidence-based diagnosis and management guidelines, the National Heart, Lung, and Blood Institute (NHLBI) Expert Panel report (USA). *Haemophilia* 14:171–232, 2008.

[30]Oh, K. W., K. Lee, B. Ahn, and E. P. Furlani. Design of pressure-driven microfluidic networks using electric circuit analogy. *Lab Chip* 12:515, 2012.

[31]Okorie, U. M., W. S. Denney, M. S. Chatterjee, K. B. Neeves, and S. L. Diamond. Determination of surface tissue factor thresholds that trigger coagulation at venous and arterial shear rates: amplification of 100 fM circulating tissue factor requires flow. *Blood* 111:3507–3513, 2008.

[32]Onasoga-Jarvis, A. A., T. J. Puls, S. K. O'Brien, L. Kuang, H. J. Liang, and K. B. Neeves. Thrombin generation and fibrin formation under flow on biomimetic tissue factor-rich surfaces. *J. Thromb. Haemost*. 12:373–382, 2014.

[33]Pries, A. R., B. Reglin, and T. W. Secomb. Remodeling of blood vessels: responses of diameter and wall thickness to hemodynamic and metabolic stimuli. *Hypertension* 46:725–731, 2005.

[34]Pries, A. R., D. Neuhaus, and P. Gaehtgens. Blood viscosity in tube flow: dependence on diameter and hematocrit. *Am. J. Physiol*. 263:H1770–H1778, 1992.

[35]Rana, K., and K. B. Neeves. Blood flow and mass transfer regulation of coagulation. *Blood Rev*. 2016. doi: 10.1016/j.blre.2016.04.004.

[36]Reininger, A. J., I. Bernlochner, S. M. Penz, C. Ravanat, P. Smethurst, R. W. Farndale, C. Gachet, R. Brandl, and W. Siess. A 2-step mechanism of arterial thrombus formation induced by human atherosclerotic plaques. *J. Am. Coll. Cardiol*. 55:1147–1158, 2010.

[37]Ruggeri, Z. M. Platelet adhesion under flow. *Microcirculation* 16:58–83, 2009.

[38]Savage, B., F. Almus-Jacobs, and Z. M. Ruggeri. Specific synergy of multiple substrate-receptor interactions in platelet thrombus formation under flow. *Cell* 94:657–666, 1998.

[39]Schneider, C. A., W. S. Rasband, and K. W. Eliceiri. NIH Image to ImageJ: 25 years of image analysis. *Nat. Methods* 9:671–675, 2012.

[40]Sylman, J. L., D. T. Artzer, K. Rana, and K. B. Neeves. A vascular injury model using focal heat-induced activation of endothelial cells. *Integr. Biol*. 7:801–814, 2015.

[41]Tovar-Lopez, F. J., G. Rosengarten, E. Westein, K. Khoshmanesh, S. P. Jackson, A. Mitchell, and W. S. Nesbitt. A microfluidics device to monitor platelet aggregation dynamics in response to strain rate micro-gradients in flowing blood. *Lab Chip* 10:291, 2010.

[42]Tsai, M., A. Kita, J. Leach, R. Rounsevell, J. N. Huang, J. Moake, R. E. Ware, D. A. Fletcher, and W. A. Lam. In vitro modeling of the microvascular occlusion and thrombosis that occur in hematologic diseases using microfluidic technology. *J. Clin. Invest*. 122:408–418, 2011.

[43]Turitto, V. T., H. J. Weiss, and H. R. Baumgartner. Platelet interaction with rabbit subendothelium in von Willebrand's disease: altered thrombus formation distinct from defective platelet adhesion. *J. Clin. Invest*. 74:1730–1741, 1984.

[44]Valentino, L. A. Blood-induced joint disease: the pathophysiology of hemophilic arthropathy. *J. Thromb. Haemost*. 8:1895–1902, 2010.

[45]Valentino, L. A., N. Hakobyan, T. Kazarian, K. J. Jabbar, and A. A. Jabbar. Experimental haemophilic synovitis: rationale and development of a murine model of human factor VIII deficiency. *Haemophilia* 10:280–287, 2004.

[46]van der Meijden, P. E. J., I. C. A. Munnix, J. M. Auger, J. W. P. Govers-Riemslag, J. M. E. M. Cosemans, M. J. E. Kuijpers, H. M. Spronk, S. P. Watson, T. Renné, and J. W. M. Heemskerk. Dual role of collagen in factor XII-dependent thrombus formation. *Blood* 114:881–890, 2009.

[47]van Gestel, M. A., J. W. M. Heemskerk, D. W. Slaaf, V. V. T. Heijnen, S. O. Sage, R. S. Reneman, and M. G. A. Oude Egbrink. Real-time detection of activation patterns in individual platelets during thromboembolism in vivo: differences between thrombus growth and embolus formation. *J. Vasc. Res*. 39:534–543, 2002.

[48]van Gestel, M. A., S. Reitsma, D. W. Slaaf, V. V. T. Heijnen, M. A. H. Feijge, T. Lindhout, M. A. M. J. van Zandvoort, M. Elg, R. S. Reneman, J. W. M. Heemskerk, and M. G. A. Oude Egbrink. Both ADP and thrombin regulate arteriolar thrombus stabilization and embolization, but are not involved in initial hemostasis as induced by micropuncture. *Microcirculation* 14:193–205, 2007.

[49]Van Kruchten, R., J. M. E. M. Cosemans, and J. W. M. Heemskerk. Measurement of whole blood thrombus formation using parallel-plate flow chambers—a practical guide. *Platelets* 23:229–242, 2012.

[50]Versteeg, H. H., J. W. M. Heemskerk, M. Levi, and P. H. Reitsma. New fundamentals in hemostasis. *Physiol Rev* 93:327–358, 2013.

[51]Weisel, J. Fibrinogen and fibrin. *Adv. Protein Chem*. 70:248–299, 2005.

[52]Westein, E., A. D. van der Meer, M. J. E. Kuijpers, J.-P. Frimat, A. van den Berg, and J. W. M. Heemskerk. Atherosclerotic geometries exacerbate pathological thrombus formation poststenosis in a von Willebrand factor-dependent manner. *Proc. Natl. Acad. Sci*. 110:1357–1362, 2013.

[53]Westrick, R. J., M. E. Winn, and D. T. Eitzman. Murine models of vascular thrombosis. *Arterioscl. Throm. Vas*. 27:2079–2093, 2007.

[54]Young, M. E., P. A. Carroad, and R. L. Bell. Estimation of diffusion coefficients of proteins. *Biotechnol. Bioeng*. 22:947–955, 1980.

[55]Zheng, Y., J. Chen, M. Craven, N. W. Choi, S. Totorica, A. Diaz-Santana, P. Kermani, B. Hempstead, C. Fischbach-Teschl, J. A. López, and A. D. Stroock. In vitro microvessels for the study of angiogenesis and thrombosis. *Proc. Natl. Acad. Sci*. 109:9342–9347, 2012.